# The acoustic diversity of the seabed based on the similarity index computed from Chirp seismic data

Gwang H. Lee, Han J. Kim, Dae C. Kim, Bo Y. Yi, Seong M. Nam, Boo K. Khim, and Moon S. Lim

Lee, G. H., Kim, H. J., Kim, D. C., Yi, B. Y., Nam, S. M., Khim, B. K., and Lim, M. S. 2009. The acoustic diversity of the seabed based on the similarity index computed from Chirp seismic data. – ICES Journal of Marine Science, 66: 227–236.

The similarity index (SI), computed from the singular value decomposition of seabed-echo envelopes recorded in Chirp seismic data, was tested in mapping the acoustic diversity of the seabed in Suyong Bay, Busan, Korea. Rocky bottom is characterized by low SI values, indicating acoustic heterogeneity, and sedimentary seabed by high SI values, also indicating acoustic homogeneity. Isolated areas of low SI values, not identified as rocky bottom in Chirp profiles, may suggest a shallow basement. The gradual seaward change of the substratum from coarse-grained to relatively poorly sorted, finer-grained sediments also corresponds to an overall seaward decrease in the SI value. The straightforward and quick computation of the SI makes it possible to assess the gross acoustic diversity of the seabed in almost real time.

**Keywords:** acoustic seabed classification, Chirp seismic data, similarity index, singular value decomposition.

Received 15 March 2008; accepted 30 July 2008; advance access publication 8 September 2008.

*G. H. Lee, D. C. Kim, B. Y. Yi, and S. M. Nam: Department of Environmental Exploration Engineering, Pukyong National University, Busan 608-737, Korea. H. J. Kim: Korea Ocean Research and Development Institute, Ansan 426-744, Korea. B. K. Khim: Division of Earth Environmental System, Pusan National University, Busan 609-735, Korea. M. S. Lim: Geo-Marine Technology, Busan 608-020, Korea. Correspondence to G. H. Lee: tel: +82 51 6296558; fax: +82 51 6296553; e-mail: gwanglee@pknu.ac.kr.*

## Introduction

Textural, physical, and geotechnical properties of seabed sediments are basic data in many areas of science and engineering, including marine geology and geophysics, acoustics, environmental science, ocean and civil engineering, and fisheries. The most commonly used method for determining sediment texture is grab sampling or coring from a stationary vessel, followed by laboratory analyses. This method, however, not only fails to obtain undisturbed samples but is also extremely slow and expensive and mostly blind, and provides information only at discrete sites.

In recent years, considerable effort has been expended on the remote classification of seabed sediments using acoustic tools such as single-beam echosounders, multibeam and sidescan sonar, and sub-bottom profilers. The shape of the seabed echo recorded by an echosounder depends largely on the roughness or the texture of the seabed, which affects the degree of backscatter (Quester Tangent Corporation, 1997; Hamilton *et al.*, 1999; Ellingsen *et al.*, 2002; Lied *et al.*, 2004). The early part of a seabed echo is a peak dominantly from a specular return, and the tail behind it is principally from incoherent backscatter (Hamilton *et al.*, 1999; Van Walree *et al.*, 2005). Therefore, the length and the energy of the tail can provide information about the acoustic roughness of the seabed (Hamilton, 2001). Acoustic penetration into the seabed and the presence of subsurface reflectors can also affect the shape of the echo through volume-scattering (Hamilton, 2001).

The shape of an echo is also a function of hardness and frequency, ping length, and the beam width of the echosounder (Hamilton *et al.*, 1999). An echosounder is inexpensive and can be operated easily from virtually any type of vessel. However, the output from the echosounder requires considerable interpolation to generate a seabed map with 100% coverage (Kenny *et al.*, 2003). Acoustic seabed classification systems (e.g. QTC View) using echosounders are based on unknown parameters and proprietary algorithms, so users are reliant on manufacturers for improvements and upgrades (Hamilton, 2001). Moreover, the parameters are often system-dependent.

Backscatter strength and the image texture of sidescan and multibeam sonar data can provide some information about seabed type (De Moustier and Matsumoto, 1993; Huvenne *et al.*, 2002; Collier and Brown, 2005). The advantage of such systems is their rapid coverage of a large area of seabed. A sidescan sonar is affordable and relatively easy to operate from a range of vessels, whereas a multibeam sonar is a more-complicated system and expensive to operate. The information from these systems available for analysis is backscatter intensity, which alone is not generally able to characterize seabed type, as deduced from echosounder data (Hamilton, 2001). The output from sidescan and multibeam sonar also requires considerable post-processing time and expense to obtain appropriate seabed classification (Kenny *et al.*, 2003).

Data from sub-bottom profilers such as the Chirp profiling system have also been used for seabed classification (LeBlanc *et al.*, 1992; Schock and LeBlanc, 1992; Kim *et al.*, 2002; Stevenson *et al.*, 2004). Acoustic impedance and attenuation profiles produced from Chirp data can be used to classify seabed sediments and to predict sediment physical properties (Schock and LeBlanc, 1992; Panda *et al.*, 1994). For low-frequency (e.g. 2–7 kHz) acoustic signals recorded in the Chirp system

(J. Tegowski, pers. comm., 2008), a considerable part of the return signal comes from volume-scattering at sediment inhomogeneities (Jackson and Biggs, 1992). Kim *et al.* (2002) applied the Karhunen–Loève (KL) transform to Chirp data to compute a similarity index (SI), which is the percentage of the energy of the coherent part contained in the bottom-return signals. The SI appears to represent the variation of the seabed in terms of bottom roughness, or sediment volume heterogeneity, or a mixture of both factors. The disadvantage of sub-bottom profilers is that, like echosounders, they require extensive ground-truth data and spatial interpolation between tracks to discriminate between different seabed types.

For this work, we applied the SI method to Chirp data in standard SEG-Y format, acquired from Suyong Bay (Figure 1), Busan, Korea. SI values were compared with sidescan-sonar images, Chirp profiles, and ground-truth data from a number of sediment-grab samples. We show in the following sections that SI values can provide valuable information on the gross acoustic diversity of the seabed and thus help to differentiate between substrata of different sediment type.

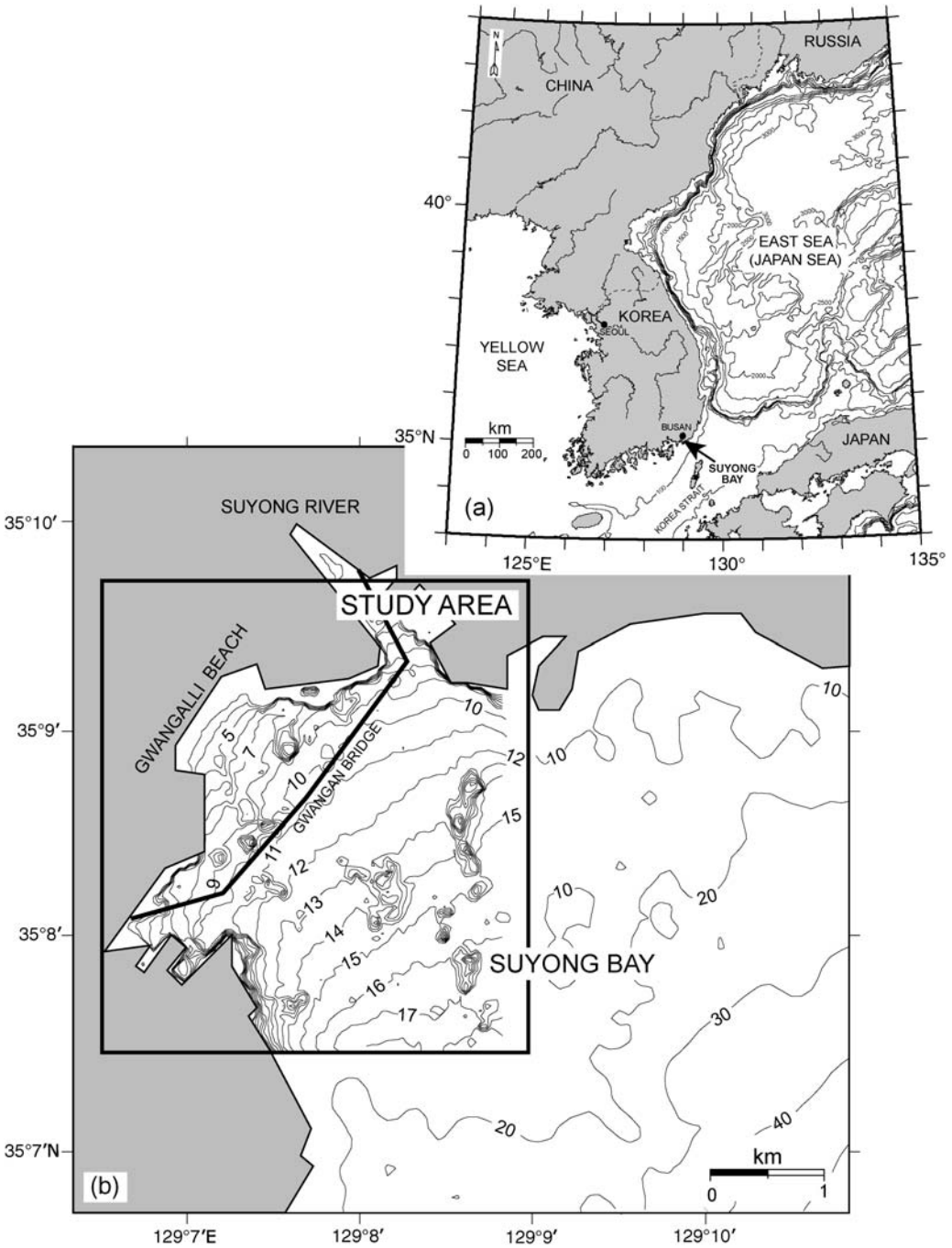


**Figure 1.** (a) Physiographic map of the Korean Peninsula and surrounding seas, and (b) a bathymetric map of Suyong Bay. The bathymetric data of the study area were provided by the National Oceanographic Research Institute of Korea. Contours are in metres.

## Background: the SI

The KL transform or reconstruction technique produces orthogonal principal components from digital data and has been used widely in seismic data analysis and digital-image processing (Mallick and Murthy, 1984; Jones and Levy, 1987; Freire and Ulrych, 1988). Freire and Ulrych (1988) implemented the KL transform for the singular-value decomposition (SVD), to extract information from seismic-reflection data. The first few eigenimages or SVD descriptions obtained from decomposition of the input data matrix contain the contributions from horizontally coherent seismic signals.

Let $S$ be a seismic-reflection data matrix containing $N$ traces each with $M$ sampling points:

$$S = \{s_{ij}\},\ i = 1, 2, \ldots, M;\ j = 1, 2, \ldots, N. \tag{1}$$

The SVD of $S$ is given by

$$S = \sum_{i=1}^{r} \sigma_i U_i V_i^{\mathrm{T}}, \tag{2}$$

where the superscript T means a transpose, $r$ the rank of $S$, $U_i$ the $i$th eigenvector of $SS^{\mathrm{T}}$, $V_i$ the $i$th eigenvector of $S^{\mathrm{T}}S$, and $\sigma_i$ the $i$th singular value of $S$. The singular values $\sigma_i$ are the positive square roots of the eigenvalues of the covariance matrices $SS^{\mathrm{T}}$ and $S^{\mathrm{T}}S$. The factor $U_iV_i^{\mathrm{T}}$ in Equation (2) is an $(M \times N)$ matrix of unit norm or the $i$th eigenimage of $S$.

The most influential contributions in the presentation of $S$ are from the first few eigenimages, because the singular values are ordered in decreasing amplitude. Therefore, if $S$ is composed of traces with a high degree of trace-to-trace correlation, it may be reconstructed from just the first few eigenimages. Reconstruction using the first few singular values is known as principal component construction, whereas that using the remaining singular values is known as misfit reconstruction.

Freire and Ulrych (1988) showed that the percentage of energy ($E$) contained in a reconstructed image is given by

$$E = \frac{\sum_{i=p}^{q} \sigma_i^2}{\sum_{i=p}^{r} \sigma_i^2}, \quad 1 \le p \le q \le r. \tag{3}$$

The choice of $p$ and $q$ depends on the relative magnitudes of the singular values, which are a function of the input data.

Milligan *et al.* (1978) showed that the largest characteristic root of the covariance matrix in the SVD accounts for 97% of the observed variance. Therefore, almost all the pure reflectivity at the seabed can be reconstructed from the first principal component. Consequently, the first eigenimage, reconstructed from the SVD of a set of adjacent traces, contains the coherent return signal from the seabed. Kim *et al.* (2002) proposed the SI, by taking $q = 1$ in Equation (3) as a measure of the coherence of the seabed reflections of adjacent traces:

$$\mathrm{SI} = \frac{\sigma_1^2}{\sum_{i=p}^{r} \sigma_i^2}. \tag{4}$$

SI values range from 0 to 1 for various seabed conditions, and increase with the increasing acoustic homogeneity of the seabed. Low SI values indicate textural inhomogeneity and

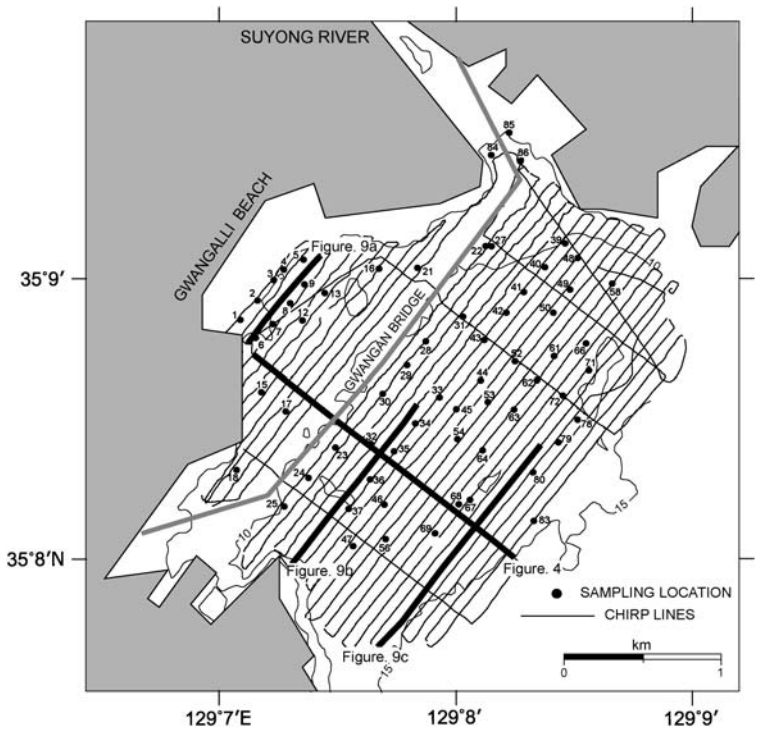


**Figure 2.** Chirp data tracklines and grab-sampling locations. Thick lines indicate the Chirp profiles shown in other Figures (numbers shown here). Contours are water depth in metres.

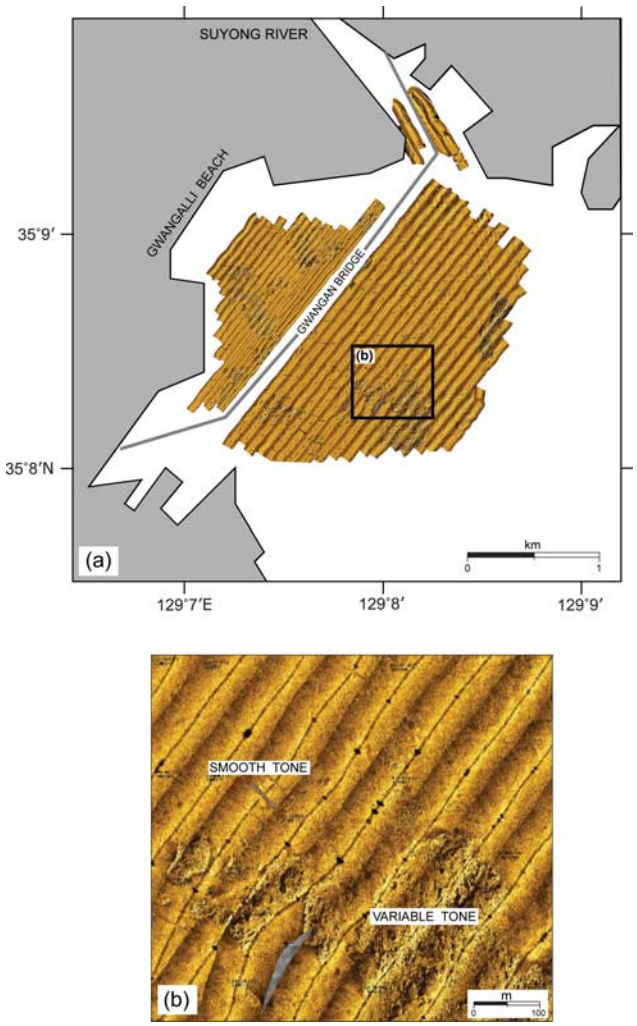


**Figure 3.** (a) Mosaicked sidescan-sonar images of the study area, and (b) a close-up of a sidescan-sonar image. Smooth and weak-to-moderate tone corresponds to sedimentary seabed, and dark and variable tone to rocky bottom.

**Table 1.** Mean grain size (φ) and sorting (φ) of sediment-grab samples.

| Site | Mean (φ) | Sorting (φ) |
|---|---|---|
| 1 | 3.3 | 2.1 |
| 2 | 3.99 | 2.04 |
| 3 | 3.42 | 2.28 |
| 4 | 3.71 | 1.86 |
| 5 | 4.89 | 2.78 |
| 6 | 3.62 | 1.85 |
| 7 | 3.72 | 2.01 |
| 8 | 3.61 | 1.96 |
| 9 | 3.38 | 1.66 |
| 12 | 4.2 | 2.6 |
| 13 | 3.6 | 3.05 |
| 15 | 3.97 | 2.01 |
| 16 | 3.83 | 2.23 |
| 17 | 4.09 | 1.81 |
| 18 | 4.07 | 2.02 |
| 21 | 4.18 | 2.1 |
| 22 | 5.27 | 2.27 |
| 23 | 4.11 | 2.75 |
| 24 | 3.99 | 1.98 |
| 25 | 3.65 | 2.31 |
| 27 | 4.41 | 2.64 |
| 28 | 4.6 | 2.94 |
| 29 | 4.53 | 1.94 |
| 30 | 4.27 | 1.67 |
| 31 | 6.28 | 2.35 |
| 32 | 4.59 | 2.01 |
| 33 | 4.83 | 2.58 |
| 34 | 4.06 | 1.96 |
| 35 | 4.15 | 2.19 |
| 36 | 3.99 | 1.91 |
| 37 | 4.32 | 2.52 |
| 39 | 3.94 | 2.9 |
| 40 | 6.17 | 1.95 |
| 41 | 4.71 | 2.7 |
| 42 | 5.59 | 2.71 |
| 43 | 3.61 | 2.51 |
| 44 | 4.11 | 2.41 |
| 45 | 4.12 | 2.15 |
| 46 | 4.7 | 2.48 |
| 47 | 4.9 | 2.17 |
| 48 | 5.12 | 2.92 |
| 49 | 5.39 | 2.91 |
| 50 | 6.04 | 2.93 |
| 52 | 4.51 | 2.87 |
| 53 | 4.59 | 2.39 |
| 54 | 5.1 | 2.74 |
| 56 | 4.56 | 2.07 |
| 58 | 5.47 | 1.96 |
| 61 | 2.59 | 2.64 |
| 62 | 4.06 | 2.17 |
| 63 | 5.28 | 1.92 |
| 64 | 5.92 | 1.47 |
| 66 | 3.92 | 3.13 |
| 67 | 3.47 | 2.47 |
| 68 | 4.54 | 1.92 |
| 69 | 4.7 | 2.25 |
| 71 | 7.22 | 2.24 |
| 72 | 3.49 | 3.05 |
| 78 | 2.81 | 3.42 |
| 79 | 3.6 | 1.84 |
| 80 | 5.82 | 1.99 |
| 83 | 5.19 | 2.7 |
| 84 | 3.67 | 1.63 |
| 85 | 3.51 | 1.7 |
| 86 | 3.78 | 1.96 |

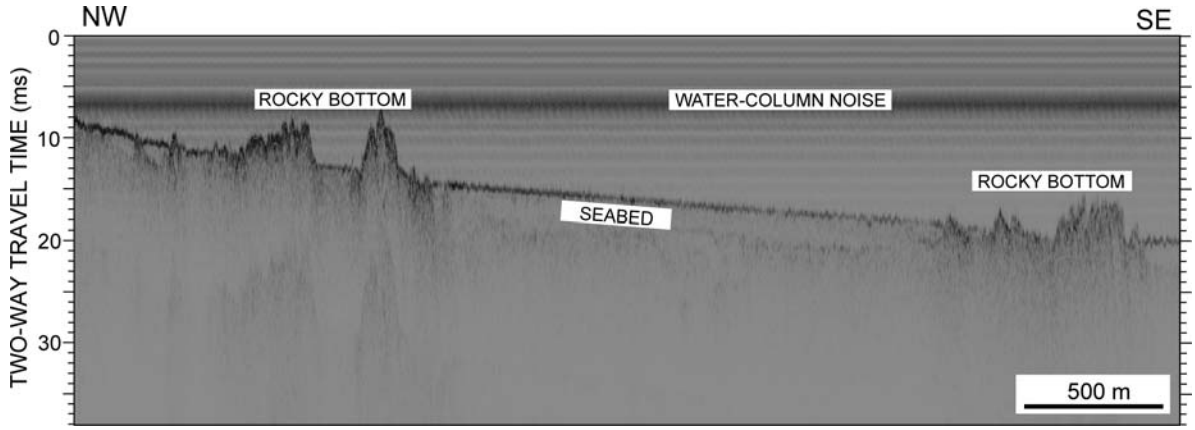


**Figure 4.** Chirp profile showing smooth sedimentary seabed and rugged rocky bottom, showing also strong water-column noise (source pulse ringing). See Figure 2 for the location.

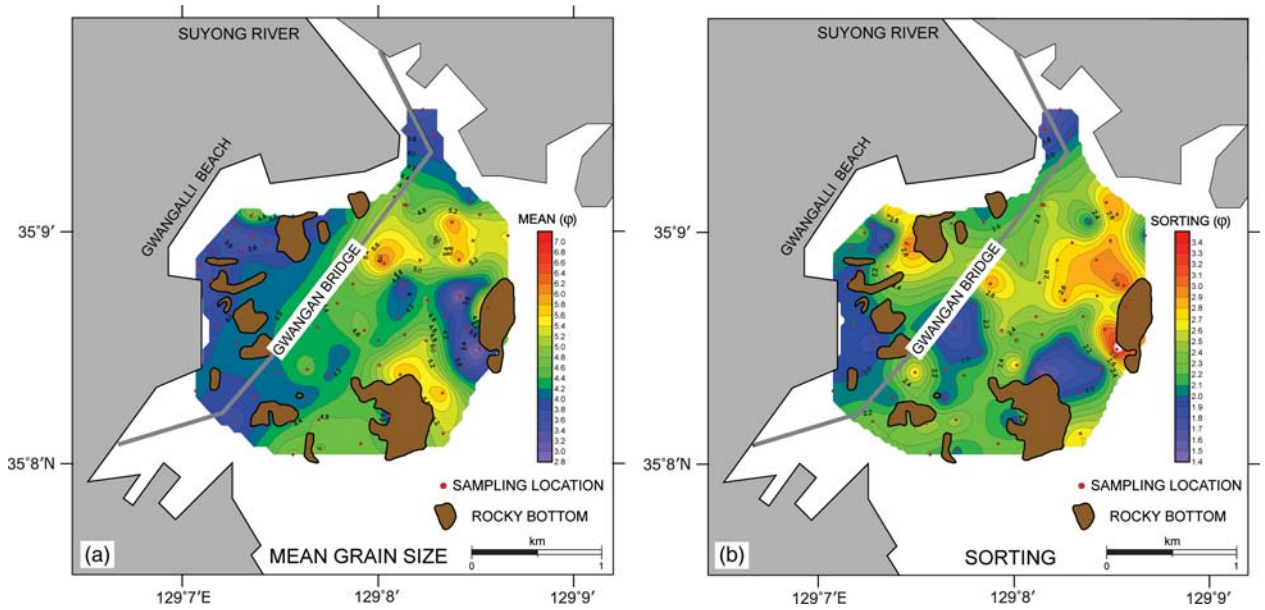


**Figure 5.** (a) Distribution of mean grain size on a scale of φ. Coarse-grained (<4.2 φ) sediments are distributed mainly near the coast, and mean grain size decreases seawards. (b) Distribution of sorting values on a φ scale. The overall distribution of sorting values is similar to that of the mean grain size. Relatively well-sorted (sorting <2.1 φ) sediments occur near the coast and less well-sorted (sorting >2.5 φ) sediments in the northern central and eastern parts of area.

great roughness. The SI is independent of ping-to-ping amplitude variations caused by extraneous factors, such as amplifier gains and spreading losses, because $S$ can be almost fully reconstructed by the first eigenimage $\sigma_1 u_1 v_1^{\mathrm{T}}$ (Kim *et al.*, 2002).

## Study area

Suyong Bay is located in the central part of Busan, Southeast Korea, and covers more than 25 km$^2$ (Figure 1). The long, ~1 km, sandy Gwangalli Beach, one of the most popular tourist beaches in Korea, forms the innermost coastline of the bay. Gwangalli Beach has been affected by erosion, and large quantities of sand are brought to the beach every year for shoreface nourishment, the sedimentological impact of which remains poorly understood. The water depth of Suyong Bay gradually increases seawards, reaching >30 m where the bay opens into the deeper Korea Strait. Silty sand is dominant near the coast and passes seawards into sandy silt (Choi, 1994). The gentle seabed of the bay is locally interrupted by exposed rocky substrata. The bay is characterized by a semi-diurnal tide with minimum and maximum tidal ranges of 0.9 and 1.2 m, respectively (Hydrographic Office of Korea, 1982). The Suyong River is the main sediment source in the area and has been urbanized, with a wide range of pollution from domestic sewage.

## Data and methods

The data used in this study were: (i) more than 4 km$^2$ of sidescan-sonar images, (ii) some 95 km of Chirp (2–7 kHz) profiles, and (iii) 65 sediment-grab samples (Figure 2). Sidescan images were

obtained using a SeaScan (S-1500DI) 400-kHz, sidescan-sonar system in March 2006. The swath width per track was ~75 m. A pattern of NE–SW orientated, parallel survey lines provides nearly complete sonar coverage in the study area (Figure 3a). Ship navigation for sidescan-sonar data acquisition was based on a differential global positioning system (DGPS) with positional accuracy of ~1 m. However, the sidescan towfish was not navigated independently of the ship. Time-varied gain was applied to the sonar data in the field to correct for transmission loss. Field data were transferred to a PC workstation for post-processing using PostScan (SeaScan, 2006). Post-processing included the standard procedures: slant-range correction, beam-angle correction, contrast normalization, geo-referencing, and mosaicking.

Chirp profiles were collected in June 2007, using the Datasonics Chirp II (CAP-6000), with 16 transducers and 2–7 kHz of sweep. The pulse length was maintained at 10 ms and the trigger rate at 0.25 s. Ship navigation for Chirp data acquisition was based on a DGPS. The field Chirp data in SEG-Y format were transferred to a PC workstation for interpretation using Kingdom Suite™ (version 8.0). Bandpass filtering and automatic gain control were applied to the Chirp data before interpretation to improve data quality.

Seabed sediments were collected by grab at 65 locations during June 2006. The grab-sampling locations were fairly evenly distributed except for the areas near and beneath Gwangan Bridge, and in the southernmost part of the area. Sediment grab sampling was initially attempted at 86 locations, based on preliminary interpretation of the bathymetric map and sidescan-sonar images, but sediments were not recovered at 21 locations that were apparently on or near the rocky seabed or covered by shells. The sediment texture of the grab samples was determined using a combination of the wet-sieve technique (Folk, 1968) and the Sedigraph method. The results from the coarse- and fine-fraction analyses were combined to give the percentage weight per phi (φ) grain-size class for each grab sample. Mean grain size and sorting (Table 1) were computed by the moment method of Folk and Ward (1957).

## Data analysis and results

Backscatter intensity of the sidescan-sonar data can be divided into two categories: (i) smooth and weak-to-moderate tone (light colours), and (ii) variable but generally dark tone (colours with variable lightness; Figure 3). The variable tone corresponds to the rocky bottom identified in the bathymetric map and Chirp profiles. The strongest backscatter intensity is over rocky bottom in the easternmost part of the area. The weak-to-moderate tone coincides largely with the smooth seabed covered by sediments. No distinct sedimentary features can be seen from the sidescan-sonar images.

The Chirp profiles reveal smooth seabed and rugged rocks or basement (Figure 4). The exposed rocks are mainly in the western and southeastern parts of the area. The height of the basement rocks from the seabed locally reaches >7 m. The central part of the area is characterized by smooth seabed, and in some areas, the rocky basement appears to be covered by a thin veneer of sediments. Overall, the Chirp penetration is limited, so the acoustic basement is not clearly recognizable except for the areas with exposed rock. No distinct depositional or erosional features are seen.

Figure 5a and b show the distribution of mean grain size and sorting, contoured using Surfer®, respectively. Coarse-grained (<4.2 φ) sediments are distributed mainly near the coast; the 4.2-φ isoline is approximately parallel to the shore. Coarse-grained sediments are also found next to the basement rocks in the eastern part of the area. Fine-grained (>5.0 φ) sediments occur in the northern, central part of the area, and between basement rocks in the southeastern part of the area. The sediments sampled are poorly (1.0–2.0 φ) to very poorly sorted (2.0–4.0 φ), according to the sorting scale of Folk (1968). The distribution of sorting values is generally similar to that of mean grain-size distribution: relatively well-sorted (sorting <2.1 φ) sediments near the coast and less well-sorted (sorting >2.5 φ) sediments in the northern, central, and eastern parts of the area.

## Computation of SI

The Datasonics Chirp II (CAP-6000) stores recorded data on disk in SEG-Y format. However, the data are not the conventional voltage or pressure time-series, but rather consist of amplitude envelopes. Envelope samples are always positive and contain no phase information (Figure 6). The advantage of envelope data is that the reflection strength can be used for visualization: their disadvantage is that phase information is absent, so the vertical resolution is relatively low and further signal processing cannot be applied easily (Romijin and Blacquière, 2001). Kim *et al.* (2002) modified their Chirp II system to record raw voltage time-series data, which were used for the computation of SI. Here, we used the envelope data despite their disadvantage, because modification of the Chirp system is not required. Also, the shapes and energies of amplitude envelopes still represent the acoustic characteristics of the seabed (Hamilton *et al.*, 1999), because amplitude envelopes have a peak from specular return and a tail from incoherent backscatter contributions.

Data editing and conditioning for the computation of the SI from Chirp data are shown in Figure 7. The Chirp data we used contain high-amplitude noises in the water column (Figure 7a) and bad records. The first step is to remove the water-column noises and bad records (Figure 7b). The algorithm for the removal of water-column noises was programmed and implemented in data processing, but bad records were removed manually. After data editing and conditioning, seabed-echo

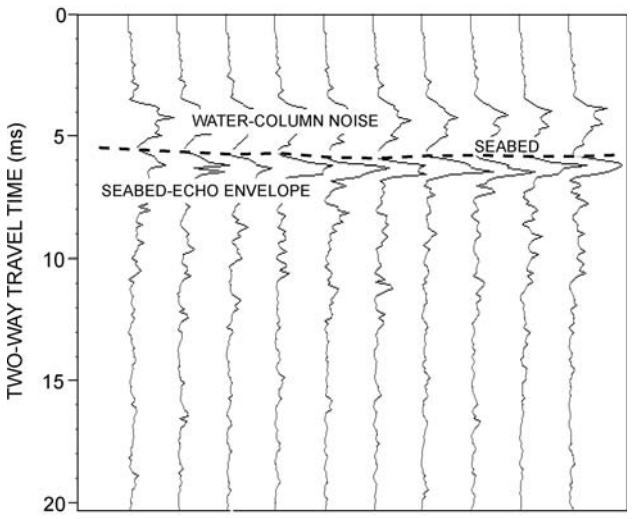


**Figure 6.** Seabed-echo envelopes with peaks and tails.

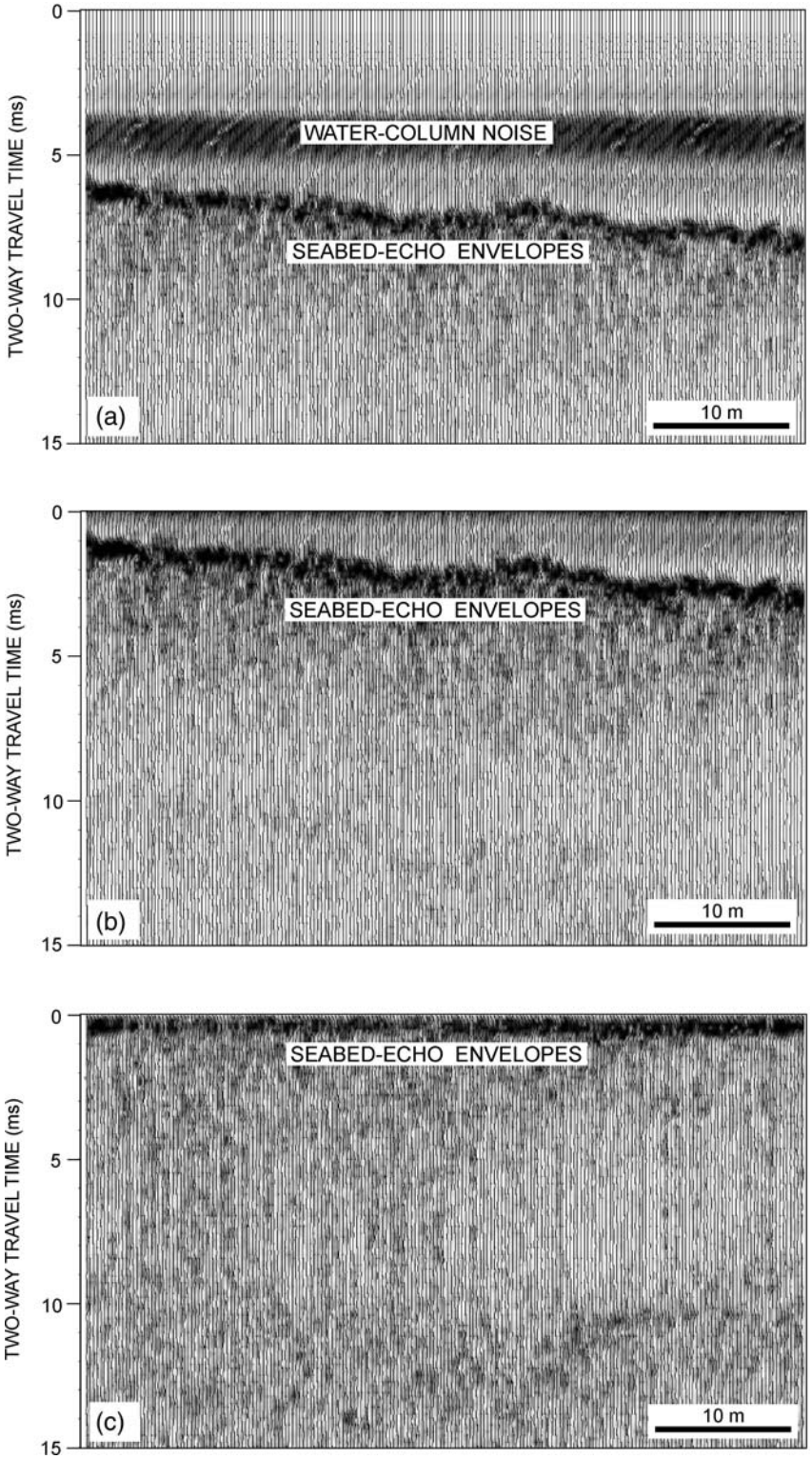


**Figure 7.** Editing and conditioning of Chirp traces for SI computation. (a) Chirp traces before editing and conditioning, and (b) Chirp traces after removal of water-column noise. (c) Seabed-echo envelopes are picked and statistically shifted to be aligned at time = 0.

envelopes were picked using the power ratio, $r$, expressed as

$$r_i = \frac{\sum_{k=0}^{k=n-1} A_{i+k}^2}{\sum_{k=0}^{k=n-1} A_{i-k}^2}, \quad (5)$$

where $r_i$ is the power ratio at the $i$th sample, $A_{i+k}$ and $A_{i-k}$ the amplitudes at the $(i+k)$th sample and $(i-k)$th sample, respectively, and $n$ the number of samples in the sliding window. The travel time for the first sample of the seabed-echo envelope is selected based on the maximum power ratio for each trace.

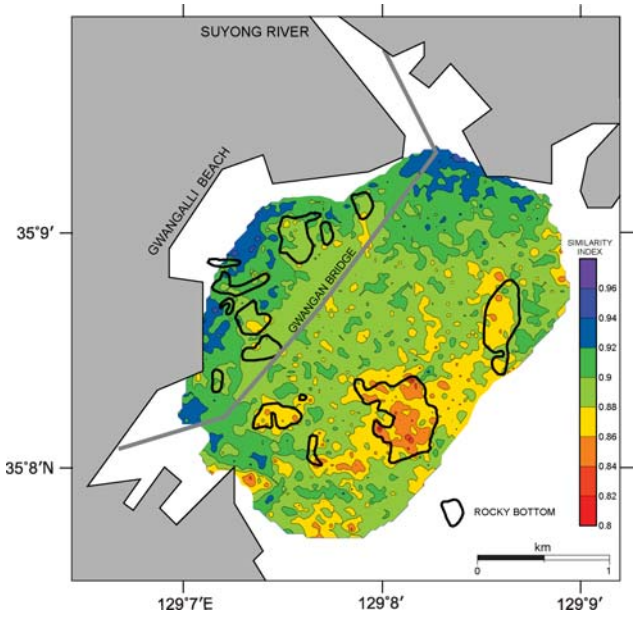


**Figure 8.** Contoured SI map. SI values range from <0.8 to >0.96. Areas of high (>0.9) SI are along the coast. Lowest (<0.86) SI values are coincident with large basement rock in the southeastern part of area. Smaller areas of low SI also occur over the exposed basement.

The number of samples in the window is three, yielding reliable firstbreak selections.

Next, the traces were statically shifted to align the seabed-echo envelopes at time = 0 for the SVD (Figure 7c). The window, sliding over echotraces, for the SVD contains nine consecutive traces 9.64-ms long, each comprising 80 samples. The computed SI was assigned to the fifth trace. The computation of SI values from any type of echotrace can be done almost instantaneously, but the completion of SI computation from the field Chirp data in this study took ~8 h because the bad records were removed manually. SI values can be computed in almost real time if the Chirp data do not contain significant numbers of bad records.

The computed SI values were smoothed by a moving-average filter of 21 data points. Then, the smoothed SI values were gridded and contoured with Surfer® (Figure 8). The gridded SI values range from <0.8 to >0.96. The areas of high (>0.9) SI values were along the coast, and the low (<0.88) values were away from the shoreface seawards of Gwangan Bridge. The lowest (<0.86) SI values were coincident with the large basement rock in the southeastern part of the area. Smaller areas of low SI values were also found over basement rocks.

## Discussion

The results of this study show that SI values can provide valuable information about the gross acoustic diversity of the seabed. SI values computed from pressure time-series (Kim *et al.*, 2002) are smallest (<0.4) over rocky substrata, increasing to ~0.6 away from those substrata, and high (~0.8) coinciding with fine sand. Therefore, the overall pattern of SI response to seabed types in our study is similar to that of Kim *et al.* (2002), although the ranges of SI values differ. The higher values and the narrow range of SI in our study can probably be attributed to the absence of phase information in the envelope data and therefore its lower resolution compared with the pressure time-series. Nevertheless, the SI values computed from the seabed-echo envelope generally agree with seabed texture. Relatively well-sorted, coarse-grained (<~4.2 φ) sediments along the coast are largely characterized by high and smoothly varying (>0.9) SI values (Figure 9a). Subsurface reflections are hardly recognizable below these coarse-grained sediments in Chirp profiles. Fine-grained sediments in much of the central part of the area exhibit intermediate (0.88–0.9) and more variable SI values (Figure 9b) than coarse-grained sediments. Weak subsurface reflections were evident below these sediments.

The rocky substrata in the southeastern part of the area are characterized by low (<0.86) SI values. The largest basement rock in the southeastern part of the area is particularly well defined by very low values of SI (Figure 9c). The exposed basement rocks near the shoreface, on the other hand, do not exhibit distinctly low SI values, but are also outlined by areas of relatively low SI. The areas surrounding the rocky seabed are associated with relatively low values (<0.88) of SI, which probably define the transition zone from the rugged rocky substrata to sediments. Isolated areas of low SI values that are not identified as exposed rocks in Chirp profiles may suggest a shallow basement.

Because seabed sediments are mostly heterogeneous and random, blind sampling can lead to the loss of important seabed information. Once the acoustic diversity of the seabed in an area is known, sediment sampling can be directed to the different areas believed to be more representative. Computation of the SI from seabed-echo envelopes of Chirp data is straightforward and quick, which makes it possible to interpret the seabed in the survey area in almost real time and allows a larger area to be surveyed in a given time if required.

The shape of the seabed-echo envelope recorded in Chirp data depends not only on the roughness and hardness of the seabed and the heterogeneities of the first few metres of sediment, but also on other physical or biotic seabed characteristics, or a combination of both. Various data-acquisition parameters can also affect the seabed echo. Therefore, we do not know which seabed properties are reflected in the SI. The accurate acoustic-penetration depths in different seabed types are also unknown, so the utility of the SI and other acoustic methods in seabed classification depends on the quantity and quality of ground-truth data. Hence, acoustic methods may not be suitable for stand-alone usage, but can serve as useful tools for filling in gaps and identifying representative areas for sediment sampling (Hamilton *et al.*, 1999).

## Conclusions

Our study has, we believe, shown that SI values computed from seabed-echo envelopes recorded by the Chirp profiling system can provide information about gross differences between substrata. The SI values reveal the areas with a marked change in seabed type, from sediment to rock. The gradual seaward change in substratum from coarse-grained to relatively poorly-sorted, finer-grained sediments also corresponds to an overall seaward decrease in the value of SI. The computation of SI is straightforward and quick, so the gross acoustic diversity of a seabed can be interpreted in almost real time from SI values. This makes the SI particularly useful for coastal and nearshore surveys, for which real-time seabed mapping is important.

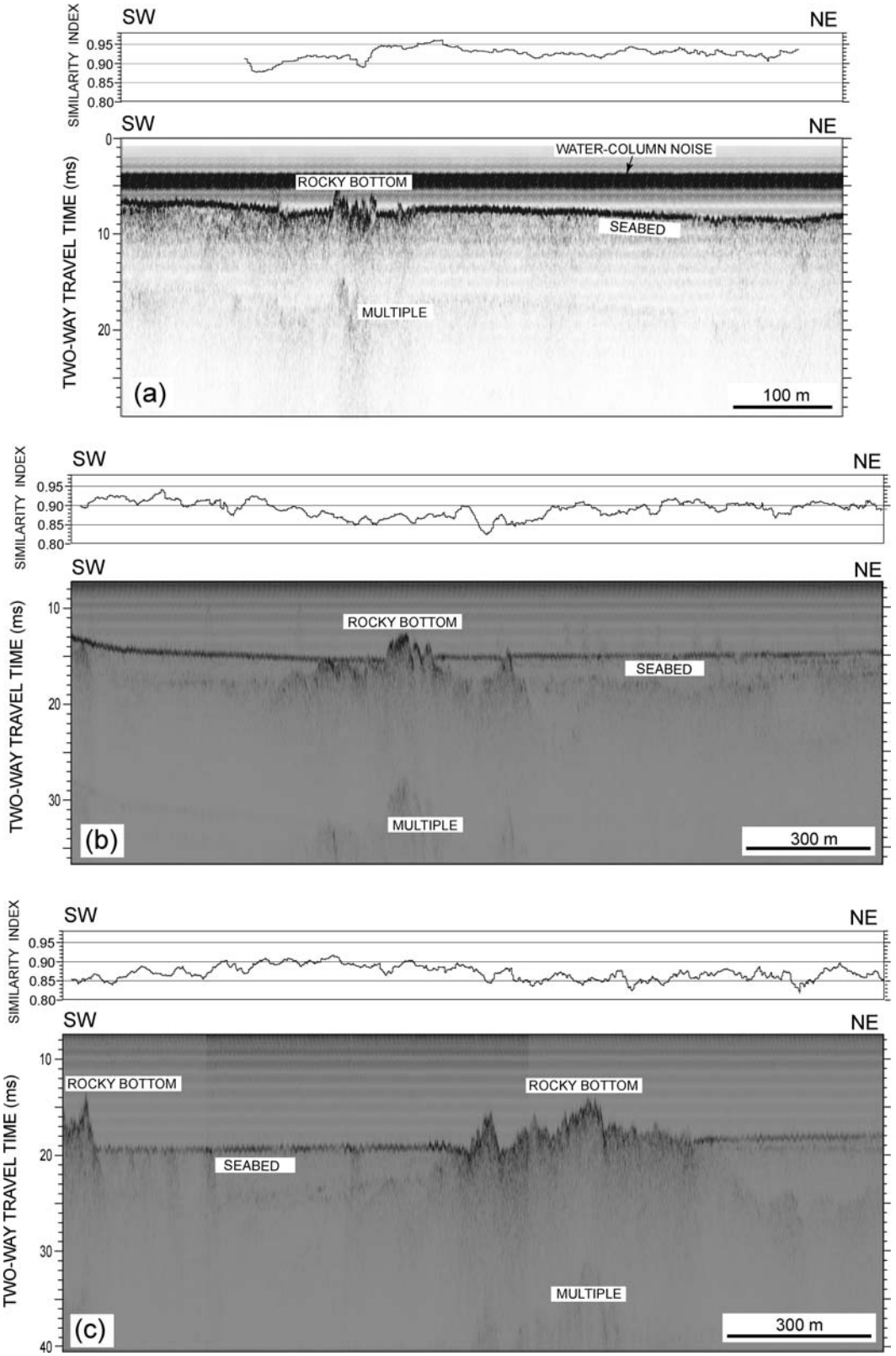


**Figure 9.** (a) Chirp profile from near the coast where relatively well-sorted, coarse-grained sediments dominate. SI values are high ($>0.9$) and evenly varying across the profile. Subsurface reflections are not recognizable. (b) Chirp profile from the central part of the area dominated by finer-grained sediments. SI values are intermediate (0.88–0.9) and more variable compared with the coarse-grained sediments. Weak subsurface reflections can be seen. (c) Chirp profile crossing the rocky bottom in the southeastern part of area. The rocky bottom is characterized by very low ($<0.86$) SI values. The areas surrounding it are associated with relatively low ($<0.88$) SI values, probably defining the transition zone from rugged rocky bottom to sediments. See Figure 2 for the location.

## Acknowledgements

We thank the National Oceanographic Research Institute of Korea for providing bathymetric data for the study area, and the reviewers Jaroslaw Tegowski and Michael Richardson for helpful comments. The research was supported by a project grant (YSG-RC0505) from Yeongnam Sea Grant, Korea. Kingdom Suite™, provided by Seismic Micro-Technology, Inc., was used to analyse and interpret the Chirp data. The similarity index was computed at the Marine Environment and Characteristics Division of the Korea Ocean Research and Development Institute (PE98050).

## References

Choi, G. Y. 1994. Geochemical characteristics of the seabed sediments in Suyong Bay, Busan. MSc thesis, Pusan National University (in Korean).

Collier, J. S., and Brown, C. J. 2005. Correlation of sidescan backscatter with grain size distribution of surficial seabed sediments. Marine Geology, 214: 431–449.

De Moustier, C., and Matsumoto, H. 1993. Seafloor acoustic remote sensing with multibeam echosounders and bathymetric sidescan sonar systems. Marine Geophysical Research, 15: 27–42.

Ellingsen, K. E., Gray, J. S., and Bjørnbom, E. 2002. Acoustic classification of seabed habitats using the QTC VIEW™ system. ICES Journal of Marine Science, 59: 825–835.

Folk, R. L. 1968. Petrology of Sedimentary Rocks. Hemphills, Austin, TX.

Folk, R. L., and Ward, W. C. 1957. A study on the significance of grain-size parameters. Journal of Sedimentary Petrology, 17: 3–27.

Freire, S. L. M., and Ulrych, T. J. 1988. Application of singular value decomposition to vertical, seismic profiling. Geophysics, 35: 591–600.

Hamilton, L. J. 2001. Acoustic Seabed Classification Systems. Defense, Science and Technology Organization of Australia.

Hamilton, L. J., Mulhearn, P. J., and Poeckert, R. 1999. Comparison of RoxAnn and QTC-view acoustic bottom classification system performance for the Cairns area, Great Barrier Reef, Australia. Continental Shelf Research, 19: 1577–1597.

Huvenne, V. A. I., Blondel, P., and Henriet, J. P. 2002. Textural analysis of sidescan sonar imagery from two mound provinces in the Porcupine Seabight. Marine Geology, 189: 323–341.

Hydrographic Office of Korea. 1982. Tidal Currents Map (Busan-Yeosu). Hydrographic Office of Korea Map Series 1420 (in Korean).

Jackson, D. R., and Biggs, K. B. 1992. High-frequency bottom backscattering: roughness versus sediment volume scattering. Journal of the Acoustical Society of America, 92: 962–977.

Jones, I. F., and Levy, S. 1987. Signal-to-noise ratio enhancement in multichannel seismic data via the Karhunen–Loeve transformation. Geophysical Prospecting, 35: 12–32.

Kenny, A. J., Cato, I., Desprez, M., Fader, G., Schüttenhelm, R. T. E., and Side, J. 2003. An overview of seabed-mapping technologies in the context of marine habitat classification. ICES Journal of Marine Science, 60: 411–418.

Kim, H. J., Chang, J. K., Jou, H. T., Park, G. T., Suk, B. C., and Kim, G. Y. 2002. Seabed classification from acoustic profiling data using the similarity index. Journal of the Acoustical Society of America, 111: 794–799.

LeBlanc, L. R., Mayer, L., Rufino, M., Schock, S. G., and King, J. 1992. Marine sediment classification using the chirp sonar. Journal of the Acoustical Society of America, 91: 107–115.

Lied, T. T., Walday, M., Olsgard, F., Ellingsen, K. E., and Holm, S. 2004. SEABEC—a single beam echosounder, seabed classification system. Oceans 2004 MTTS/IEEE Techno-Ocean 2004, 4: 2024–2028.

Mallick, K., and Murthy, Y. V. S. 1984. Pattern of Landsat MSS data over Zawar lead-zinc mines, Rajasthan, India. First Break, 2: 16–21.

Milligan, S. D., LeBlanc, L. R., and Middleton, F. H. 1978. Statistical grouping of acoustic reflection profiles. Journal of the Acoustical Society of America, 64: 795–807.

Panda, S., LeBlanc, L. R., and Schock, S. G. 1994. Sediment classification based on impedance and attenuation estimation. Journal of the Acoustical Society of America, 96: 3022–3035.

Quester Tangent Corporation. 1997. QTC View: Operator's Manual and Reference. Quester Tangent Corporation, Sidney, Canada.

Romijin, R., and Blacquière, G. 2001. Data processing of X-Star sub-bottom profiler data. The Hydrographic Journal, 101 (July). http://www.hydrographicsociety.org/Articles/journal/2001/101-3.htm (last accessed August 2007).

Schock, S. G., and LeBlanc, L. R. 1992. Sediment classification using the Chirp sonar. *In* Proceedings of the 24th Annual Offshore Technology Conference, Houston, TX, pp. 363–368.

SeaScan. 2006. PostScan User's Manual. SeaScan, Daejon, Korea.

Stevenson, I. R., McCann, C., and Runciman, P. B. 2004. An attenuation-based, sediment classification technique using Chirp sub-bottom profiler data and laboratory acoustic analysis. Marine Geophysical Research, 23: 277–298.

Van Walree, P. A., Tegowski, J., Laban, C., and Simons, D. G. 2005. Acoustic seafloor discrimination with echo shape parameters: a comparison with the ground truth. Continental Shelf Research, 25: 2273–2293.

doi:10.1093/icesjms/fsn142